IRSTI 29.19.01; 29.05.15 https://doi.org/10.26577/RCPh2025952

Montasir Salman Tayfor
Al-Baha University, Physics Department, Faculty of Science, Al-Baha, Saudi Arabia
e-mail: mtaifour@bu.edu.sa

ANALYTICAL SOLUTION OF THE TIME-FRACTIONAL SCHRÖDINGER EQUATION VIA DECOMPOSITION METHODS AND SERIES EXPANSIONS

Understanding quantum systems with intrinsic memory and spatial nonlocality requires mathematical models beyond the limits of classical calculus. In this work, the one-dimensional time-fractional Schrödinger equation is examined through a hybrid analytical framework combining the Aboodh transform with the Adomian Decomposition Method. This formulation enables the reconstruction of the wave function as a rapidly convergent analytical series. The fractional order (α) appears as a physically significant quantity that influences both the energy spectrum and the temporal evolution of quantum states. The theoretical outcomes are compared with optical band-gap variations observed experimentally in ZnO and Al-doped ZnO nanostructures, demonstrating that the fractional model provides a coherent correspondence between theory and measurable quantum behavior. Furthermore, the proposed approach exhibits superior stability and reduced computational effort compared with traditional Laplace and Fourier schemes, making it adaptable to a wide range of fractional quantum models.

Keywords: analytical fractional modeling, fractional Schrödinger equation, nonlocal quantum memory, Adomian decomposition method, analytical fractional modeling nechanics.

Монтасир Салман Тайфор
Әл-Баха университеті, физика кафедрасы, Әл-Баха, Сауд Арабиясы
e-mail: mtaifour@bu.edu.sa

Шредингер теңдеуінің бөлшек түрін кеңейту және қатарлар әдістерін қолдана отырып, аналитикалық шешім

Ішкі жады және кеңістіктік еместігі бар кванттық жүйелерді түсіну классикалық есептеулер шегінен тыс математикалық модельдерді қажет етеді. Бұл жұмыста бір өлшемді уақыттық-бөлшек Шредингер теңдеуі Абуд түрлендіруін Адомдық ыдырау әдісімен біріктіретін гибридті аналитикалық құрылым арқылы зерттеледі. Бұл тұжырым толқындық функцияны тез конвергентті аналитикалық қатар ретінде қалпына келтіруге мүмкіндік береді. Бөлшек реті (α) энергия спектріне де, кванттық күйлердің уақыттық эволюциясына да әсер ететін физикалық маңызды шама ретінде көрінеді. Теориялық нәтижелер ZnO және Al-легирленген ZnO наноқұрылымдарында эксперименттік түрде байқалған оптикалық жолақ аралығының вариацияларымен салыстырылады, бұл бөлшектік модель теория мен өлшенетін кванттық мінез-құлық арасында үйлесімді сәйкестікті қамтамасыз ететінін көрсетеді. Сонымен қатар, ұсынылған тәсіл дәстүрлі Лаплас және Фурье схемаларымен салыстырғанда жоғары тұрақтылықты және есептеу күшінің төмендеуін көрсетеді, бұл оны бөлшектік кванттық модельдердің кең ауқымына бейімдеуге мүмкіндік береді.

Түйін сөздер: аналитикалық бөлшектік модельдеу, ,өлшектік Шредингер теңдеуі, ;ергілікті емес кванттық жад, адомиялық ыдырау әдісі, аналитикалық бөлшектік модельдеу механикасы.

Монтасир Салман Тайфор
Университет Аль-Баха, физический факультет, Аль-Баха, Саудовская Аравия
e-mail: mtaifour@bu.edu.sa

Аналитическое решение уравнения Шредингера с дробной частью по времени с помощью методов разложения и рядовых разложений

Понимание квантовых систем с внутренней памятью и пространственной нелокальностью требует математических моделей, выходящих за рамки классического исчисления. В данной работе одномерное уравнение Шрёдингера с дробной частью по времени исследуется с помощью гибридной аналитической модели, сочетающей преобразование Абудха с методом разложения Адомиана. Эта формулировка позволяет реконструировать волновую функцию в виде быстро сходящегося аналитического ряда. Дробный порядок (α) выступает в качестве физически значимой величины, влияющей как на энергетический спектр, так и на временную эволюцию квантовых состояний. Теоретические результаты сравниваются с экспериментально наблюдаемыми изменениями оптической ширины запрещенной зоны в наноструктурах ZnO и ZnO, легированных Al, что демонстрирует, что дробная модель обеспечивает согласованное соответствие между теорией и измеримым квантовым поведением. Кроме того, предложенный подход демонстрирует превосходную стабильность и меньшие вычислительные затраты по сравнению с традиционными схемами Лапласа и Фурье, что делает его адаптируемым к широкому спектру дробных квантовых моделей.

Ключевые слова: аналитическое дробное моделирование, дробное уравнение Шрёдингера, нелокальная квантовая память, метод разложения Адомиана, аналитическое дробное моделирование механики.

1. Introduction

The extension of quantum mechanics into the fractional domain offers a deeper understanding of systems governed by memory, dissipation, and long-range temporal correlations that cannot be captured by standard formulations.

Fractional calculus provides an extended mathematical language capable of describing physical systems governed by memory and nonlocal interactions [1–4]. Unlike the traditional integer-order formulations, fractional derivatives introduce a continuous-order differentiation that captures intermediate dynamical states between purely local and fully diffusive regimes [5,6]. Such an approach allows a more realistic description of processes where the system's response depends not only on its current state but also on its entire evolution history.

Over the last decade, fractional operators have proven particularly effective in modeling anomalous diffusion, viscoelastic relaxation, and complex transport phenomena observed in condensed matter and quantum systems [7–10]. In quantum mechanics, the fractional extension of the Schrödinger framework has opened new perspectives for exploring non-Markovian evolution and long-range temporal correlations in wave dynamics [11–13]. This formulation generalizes the standard time-dependent Schrödinger equation by introducing a fractional-order derivative that regulates the rate of probability flow in time, thereby controlling the extent of quantum memory within the system [14,15].

The time-fractional Schrödinger equation (TFSE) thus serves as a bridge between classical quantum dynamics and fractional memory effects, enabling continuous transition from Markovian to non-Markovian behavior [16,17]. Despite its conceptual advantages, obtaining analytical solutions of the TFSE remains a major challenge because of the inherent nonlocality of fractional operators and the complexity of their integral kernels [18–20]. Standard analytical tools such as Laplace and Fourier transforms, or iterative perturbation techniques, often yield implicit integral representations or require heavy numerical computation to approximate the temporal behavior [21–23].

To overcome these limitations, the present study employs the Aboodh transform in conjunction with the Adomian Decomposition Method (ADM) [24–27]. The Aboodh transform simplifies the fractional time operator into an algebraic form, while the ADM systematically constructs rapidly convergent analytical series without discretization or linearization. This combined approach yields closed-form approximate solutions that preserve both mathematical rigor and physical interpretability.

The methodology is further validated through comparison with experimental data for ZnO and Al-doped ZnO nanostructures [28–31]. The fractional order (α) obtained from the analytical framework demonstrates direct correspondence with the optical band-gap variations observed in these materials, confirming that fractional calculus provides not merely a mathematical abstraction but also a physically meaningful model of real quantum behavior. The close consistency between theoretical predictions and experimental measurements emphasizes the practical significance of the fractional formalism in describing nanoscale electronic systems.

2 Preliminaries

In this section, we recall some basic definitions and tools from fractional calculus and integral transforms that will be employed in the subsequent analysis.

2.1 Fractional Derivatives

Several fractional derivatives are widely used to model memory and nonlocal effects in physical systems. Caputo fractional derivative of order $\alpha \in (0,1)$:

$$D_t^{\alpha} f(t)^C = \left(\frac{1}{\Gamma(1-\alpha)}\right)\int_0^t \frac{f'(s)}{(t-s)^{\alpha} ds}, \quad 0 < \alpha < 1. \tag{2.1}$$

Caputo–Fabrizio fractional derivative with exponential kernel:

$$D_t^{\alpha} f(t)^{CF} = \left(\frac{M(\alpha)}{1-\alpha}\right)\int_0^t f'^{(s)} \exp\left(-\left(\frac{\alpha}{1-\alpha}\right)(t-s)\right) ds, \quad 0 < \alpha < 1. \tag{2.2}$$

Atangana–Baleanu fractional derivative with Mittag–Leffler kernel:

$$D_t^{\alpha} f(t)^{AB} = \left(\frac{B(\alpha)}{1-\alpha}\right)\int_0^t f'^{(s)} E_{\alpha}\left(-\left(\frac{\alpha}{1-\alpha}\right)(t-s)^{\ \alpha}\right) ds, \quad 0 < \alpha < 1. \tag{2.3}$$

2.2 Aboodh Transform

The Aboodh transform is a useful integral transform for solving differential and fractional differential equations. For a given function $f(t)$, it is defined as:

$$A\{f(t)\}(u) = \int_0^{\infty} f(t)e^{-ut} dt, \quad u > 0. \tag{2.4}$$

Some important properties include:

Linearity:

$$\{af(t) + bg(t)\} = a\,A\{f(t)\} + b\,A\{g(t)\} \tag{2.5}$$

Transform of derivative:

$$A\{f'(t)\} = u\,A\{f(t)\} - f(0) \tag{2.6}$$

Transform of Caputo fractional derivative:

$$A\{D_t^{\alpha} f(t)^C\} = u^{\alpha} A\{f(t)\} - \sum_{\{k=0\}}^{\{n-1\}} u^{\alpha-k-1} f^k(0), \quad n-1 < \alpha < n. \tag{2.7}$$

2.3 Adomian Decomposition Method

The Adomian Decomposition Method (ADM) provides an analytical framework that constructs the solution of differential and fractional equations in the form of a rapidly convergent functional series. Unlike purely numerical methods, ADM separates the linear and nonlinear contributions explicitly, allowing the solution to be expressed as:

$$y(t) = \Sigma\,(from\ n = 0\ to\ \infty) y_n(t) \tag{2.8}$$

where each term $y_n(t)$ is determined recursively from the preceding ones.

The nonlinear term $N(y)$ is expanded in terms of Adomian polynomials, which represent the nonlinear interactions in a systematic manner:

$$N(y) = \Sigma\,(from\ n = 0\ to\ \infty) A_n,$$

$$A_n = \left(\frac{1}{n!}\right)\left(\frac{d^n}{d\lambda^n}\right) * \left[N\left(\Sigma\,(from\ k = 0\ to\ \infty)\lambda^k y_k\right)\right] \quad evaluated\ at\ \lambda = 0 \tag{2.9}$$

This recursive construction ensures analytical convergence and provides clear insight into how nonlinearities influence the evolution of the physical system. When ADM is applied together with the Aboodh transform, the integral operators are reduced to algebraic forms, which considerably simplifies the treatment of the time- fractional Schrödinger equation and yields closed-form analytical approximations without linearization.

3 Mathematical Formulation

We consider the one-dimensional time-fractional Schrödinger equation (FSE) in the Caputo sense with fractional order $\alpha \in (0,1]$:

$$i^{\alpha}\frac{\partial^{\alpha}\psi(x,t)}{\partial t^{\alpha}} = -\left(\frac{\hbar^2}{2m}\right)\frac{\partial^2\psi(x,t)}{\partial x^2} + V(x)\psi(x,t), \quad (3.1)$$

$$0 < \alpha \leq 1.$$

Here, $\psi(x,t)$ is the wave function, m the particle mass, $\hbar$ the reduced Planck constant, and $V(x)$ a prescribed potential. For $\alpha = 1$, (3.1) reduces to the classical Schrödinger equation.

3.1 Initial and Boundary Conditions

$$\psi(x,0) = \psi_0(x) \quad (3.2)$$

$$\psi(x,t) \to 0 \; as \; |x| \to \infty \quad (3.3)$$

$$\psi(0,t) = \psi(L,t) = 0. \quad (3.4)$$

It is convenient to denote the linear spatial operator:

$$\mathcal{L} := -\left(\frac{\hbar^2}{2m}\right)\frac{\partial^2}{\partial x^2} + V(x) \quad (3.5)$$

$$i^{\alpha}\partial_t^{\alpha}\psi(x,t) = \mathcal{L}\psi(x,t). \quad (3.6)$$

3.2 Special Cases of the Potential

1) Free particle ($V(x)$=0):

$$i^{\alpha}\partial_t^{\alpha}\psi(x,t) = -\left(\frac{\hbar^2}{2m}\right)\partial_x^2\psi(x,t), \quad x \in \mathbb{R}, t > 0 \quad (3.7)$$

2) Harmonic oscillator

$$V(x) = \frac{1}{2}m\omega^2x^2,$$

$$i^{\alpha}\partial_t^{\alpha}\psi(x,t) = -\left(\frac{\hbar^2}{2m}\right)\partial_x^2\psi(x,t) + \frac{1}{2}m\omega^2x^2\psi(x,t), \quad x \in \mathbb{R}, t > 0. \quad (3.8)$$

3) Infinite potential well (box) on (0,L):

$$V(x) = \{0, 0 < x < L;\ \infty, otherwise\} \Rightarrow$$

$$i^{\alpha}\partial_t^{\alpha}\psi = -\left(\frac{\hbar^2}{2m}\right)\partial_x^2\psi, \quad 0 < x < L, t > 0, \; with\ \psi(0,t) = \psi(L,t) \quad (3.9)$$

4 Mathematical Preliminaries

This section summarizes the mathematical background required for the development of the proposed fractional quantum framework. It includes concise formulations of fractional derivatives, the Aboodh transform, and the Adomian Decomposition Method (ADM), which together form the analytical foundation of the present study. Rather than repeating well-known definitions, emphasis is placed on their operational features relevant to solving the time-fractional Schrödinger equation.

4.1 Fractional Derivatives

Fractional derivatives generalize the standard differentiation operator to non-integer orders, providing a flexible mathematical representation of systems exhibiting long- term memory and spatial nonlocality. Such derivatives describe processes in which the present state depends continuously on all past states, making them particularly suitable for modeling relaxation and transport phenomena in complex physical systems. Among the various formulations proposed in the literature, the Caputo, Caputo–Fabrizio, and Atangana–Baleanu operators are the most widely employed due to their well-defined kernels and physical interpretability. Their essential forms are summarized in the following subsections.

(i) Caputo derivative: For a function $f \in C^n[a,b]$ and fractional order $\gamma \in (n-1,n), n \in N$, the Caputo derivative is given by:

$$D_C^f f(t) = \left(\frac{1}{r(n-\gamma)}\right)\int_0^t \frac{f^{(n)}(\eta)}{(t-\eta)^{(\gamma-n+1)d\eta}}t, \quad (4.1)$$

(ii) Caputo–Fabrizio derivative: For $0 < \gamma < 1$, the Caputo–Fabrizio (CF) derivative is defined as:

$$D_{CF}^{f} f(t) = \left(\frac{M(\gamma)}{1-\gamma}\right) \int_0^t f'(\eta) e^{\left\{-\left(\frac{\gamma}{1-\gamma}\right)(t-\eta)\right\} d\eta}. \quad (4.2)$$

(iii) Atangana–Baleanu–Caputo (ABC) derivative: For $0 < \gamma < 1$, the ABC derivative is expressed as:

$$D_{ABC}^{f} f(t) = \left(\frac{M(\gamma)}{1-\gamma}\right) \int_0^t f'(\eta) E_{\gamma}\left\{-\left(\frac{\gamma}{1-\gamma}\right)(t-\eta)\right\} d\eta. \quad (4.3)$$

4.2 Aboodh Transform

The Aboodh transform of a function f(t) is defined by:

$$A\{f(t)\} = \left(\frac{1}{s}\right) \int_0^{\infty} f(t)\, e^{(-st)} dt = F(s), \quad (4.4)$$

Key properties include:
Linearity:

$$A\{af(t) + bg(t)\} = aA\{f(t)\} + bA\{g(t)\}. \quad (4.5)$$

Derivative property (Caputo sense):

$$A\left\{D_{CF}^{f} f(t)\right\} = s^{\gamma} F(s) - \sum_{\{k=0\}}^{\{m-1\}} \frac{f^{(k)}(0)}{s^{\gamma-k}}, \quad (4.6)$$

$m - 1 < \gamma \leq m.$

Inverse transform:

$$f(t) = A^{-1\{F(s)\}} \quad (4.7)$$

4.3 Adomian Decomposition Method (ADM)

The Adomian Decomposition Method (ADM) offers a constructive analytical scheme for solving both linear and nonlinear fractional differential equations. In this framework, the solution is expanded as a rapidly convergent functional series whose individual components can be determined recursively:

$$u(t) = \sum_{0}^{\infty} u_{\mathrm{n}}(t) \quad (4.8)$$

Each term $u_n(t)$ represents a successive correction that incorporates the influence of the nonlinear operator $N(u)$. The nonlinear part of the equation can be expressed as a decomposition in terms of Adomian polynomials:

$$N(u) = \sum_{0}^{\infty} A_{\mathrm{n}} \quad (4.9)$$

where the coefficients A_n are defined by:

$$A_n = \left(\frac{1}{n!}\right)\left(\frac{d^n}{d\lambda^n}\right) N\left(\Sigma_{\{k=0\}}^{\infty} \lambda^k u_k\right)|_{\{\lambda=0\}} \quad (4.10)$$

This systematic construction enables ADM to handle nonlinearities without resorting to perturbation or linearization approximations. When combined with integral transforms such as the Aboodh transform ADM provides a direct analytical route for obtaining approximate yet accurate solutions to time-fractional Schrödinger and related quantum equations, ensuring convergence and preserving the essential physical structure of the problem.

5 Mathematical Model

To describe quantum systems that exhibit nonlocal temporal behavior, the present work employs a time-fractional Schrödinger equation (FSE) formulated within the framework of fractional calculus. This model extends the classical Schrödinger equation by replacing the first-order time derivative with a fractional derivative of order $\alpha \in (0,1]$, thereby introducing a tunable memory parameter that captures the non-Markovian evolution of the wave function. Such generalization allows the description of dissipative or memory-dependent quantum processes that cannot be represented within

the standard formulation

$$i^{\alpha}\frac{\partial^{\alpha}\psi(x,t)}{\partial t^{\alpha}} = -\frac{\left(\frac{\hbar^2}{2m}\right)\partial^2\psi(x,t)}{\partial x^2} + V(x)\psi(x,t),\ \ 0 < \alpha \leq 1 \quad (5.1)$$

In this representation, ψ(*x*, *t*) denotes the complex-valued wave function, m is the particle mass, ħ is the reduced Planck constant, and V(x) is the potential energy function. For α = 1, Equation (5.1) reduces to the standard time-dependent Schrödinger equation, while fractional values of α correspond to systems exhibiting long-term temporal correlations and fractional relaxation dynamics. $\psi(x,t)$ is the wave function, ħ is the reduced Planck's constant, m is the particle mass, and V(x) is the potential energy. For α=1, Equation (5.1) reduces to the classical Schrödinger equation [33].

5.1 Initial and Boundary Conditions

To ensure the well-posedness of Equation (5.1), we prescribe the following conditions:

$$\psi(x,0) = \psi_0(x) \quad (5.2)$$

Where ψ₀(x) is the initial wave function

$$\psi(x,t) \to 0 \ \ as\ |x| \to \infty \quad (5.3)$$

For bounded physical states.

5.2 Special Cases

The model can be applied to different physical potentials: Free particle:

$$V(x) = 0. \quad (5.4)$$

Harmonic oscillator:

$$V(x) = \left(\frac{1}{2}\right) m\,\omega^2 x^2 \quad (5.5)$$

where ω is the angular frequency. Infinite potential well:

$$V(x) = 0\ for\ 0 < x < L, and\ V(x) = \infty \quad (5.6)$$

Otherwise, with boundary conditions

$$\psi(0,t) = \psi(L,t) = 0$$

These cases will be considered in the subsequent analysis to demonstrate the effectiveness of the fractional approach and the Aboodh transform technique.

6 Analytical Solution via Aboodh Transform

We develop an analytical scheme for the time-fractional Schrödinger equation (FSE) using the Aboodh transform combined with the Adomian Decomposition Method (ADM). Let the spatial linear operator be

$$\mathcal{L} := -\left(\frac{\hbar^2}{2m}\right)\frac{\partial^2}{\partial x^2} + V(x)$$

And allow for a (possibly) nonlinear term N(ψ). For $0 < \alpha \leq 1$ in the Caputo sense, the model reads:

$$i^{\alpha}\ D_t^{\{\alpha,C\}}\psi(x,t) = \mathcal{L}\psi(x,t) + N(\psi(x,t)),\ \ \psi(x,0) = \psi_0(x) \quad (6.1)$$

6.1 Aboodh Transform of the FSE (Caputo case)

Applying the Aboodh transform A{·} in t and using

$$A\left\{D_t^{\{\alpha,C\}}\psi\right\} = s^{\alpha}\,A\{\psi\} - \frac{\psi_0}{s^{\{2-\alpha\}}}\ (for\ 0 < \alpha \leq 1)$$

We obtain:

$$i^{\alpha}\left[s^{\alpha}\,\Psi(s,x)-\frac{\psi_0(x)}{s^{\{2-\alpha\}}}\right]=\mathcal{L}\,\Psi(s,x)+A\{N(\psi)\}(s,x)\quad(6.2)$$

Rearranging gives a resolvent-type form suitable for ADM:

$$\Psi(s,x)=\frac{\psi_0(x)}{s^2}+i^{\{-\alpha\}}\,s^{\{-\alpha\}}\,[\mathcal{L}\,\Psi(s,x)+A\{N(\psi)\}(s,x)]\quad(6.3)$$

Taking the inverse Aboodh transform A^{−1}{·} yields the equivalent Volterra-type equation:

$$\psi(x,t)=\psi_0(x)+i^{\{-\alpha\}}\,A^{\{-1\}}\left\{s^{\{-\alpha\}}\,A\{\mathcal{L}\,\psi+N(\psi)\}\right\}(x,t)\quad(6.4)$$

6.2 Adomian Decomposition (Caputo case)

Assume a series solution

$$\psi=\Sigma_{\{n=0\}}^{\infty}\psi_n$$

and decompose the nonlinearity via Adomian polynomials,

$$N(\psi)=\Sigma_{\{n=0\}}^{\infty}A_n$$

Where An are generated from

$$\{\psi_k\}_{\{k=0\}}^{n}$$

Substituting into (6.4) and matching like orders gives:

$$\psi_{0(x,t)}=\psi_0(x)\quad(6.5)$$

$$\psi_{\{n+1\}}(x,t)=i^{\{-\alpha\}}\,A^{\{-1\}}\{\,s^{\{-\alpha\}}\,A\{\mathcal{L}\,\psi_{n(x,t)}+A_{n(x,t)}\}\},\quad n\geq 0\quad(6.6)$$

Here A_n are the Adomian polynomials corresponding to N(ψ). For example, for a cubic nonlinearity

$$N(\psi)=g|\psi|^{2\psi},A_0=g|\psi_0|^2\,\psi_0,$$

$$A_1=g(2|\psi_0|^2\,\psi_1+\psi_0^2\,\psi_1^{*}),etc$$

The linear case is recovered by setting N≡0.

Convergence of the Adomian Series

The convergence of the Adomian decomposition series can be established under standard boundedness and Lipschitz conditions. Let the nonlinear operator N(ψ) satisfy

$$\|N(\psi_1)-N(\psi_2)\|\leq L\|\psi_1-\psi_2\|$$

for a constant L > 0. Assume also that the kernel of the Aboodh transform, Kα(t), is continuous on [0, T] and integrable for every 0 < α < 1.

Define the successive terms of the decomposition as

$$\psi_{n+1}(t)=\int_0^t K\alpha(t-\tau)[\mathcal{L}\psi_n(\tau)+A_n(\tau)]d\tau$$

Taking the supremum norm on [0, T] gives

$$\|\psi_{n+1}\|\leq M(\|\mathcal{L}\|+L)\int_0^T|K\alpha(\tau)|d\tau\,\|\psi_n\|$$

Where M bounds the kernel. If the quantity

$$q=M(\|\mathcal{L}\|+L)\int_0^T|K\alpha(\tau)|\,d\tau<1$$

$$Then\frac{\|\psi_{n+1}\|}{\|\psi_n\|}\leq q<1$$

and the series

$$\sum_{n=0}^{\infty}\psi_n$$

converges absolutely by the ratio test. Thus, the decomposition sequence forms a contraction mapping in the Banach space $C([0, T])$.

Ensuring both existence and uniqueness of the fractional solution.

Analytic Conditions of the Aboodh Kernel

The analytic validity of the Aboodh transform kernel is essential to ensure that the fractional solution remains well-defined for all ($0 < \alpha < 1$). The kernel of the Aboodh transform in the Caputo sense can be expressed as:

$$K_a(t) = e^{-st} \cdot \frac{t^{\alpha-1}}{\Gamma(\alpha)}$$

which is continuous and absolutely integrable on every finite interval $t \in [0,T]$.

For any fractional order α satisfying $0 < \alpha < 1$, the kernel fulfills the following analytic properties:

1. Continuity: $K_a(t)$ is continuous on $[0, \infty)$ since both e^{-st} and $t^{\alpha-1}$ are continuous for positive t.
2. Integrability:

$$\int_0^{\infty} |K_a(t)|\, dt = \frac{1}{(s^{\alpha}\,\Gamma(\alpha))} < \infty$$

ensuring that the transform and its inverse exist and are bounded. 3. Analyticity in s: The Laplace-like structure of the kernel guarantees analyticity in the complex s-plane for $\mathrm{Re}(s) > 0$, satisfying the standard Cauchy conditions required for integral transforms. Hence, the Aboodh kernel satisfies all analytical and convergence conditions necessary for the application of the transform in the fractional domain ($0 < \alpha < 1$). This confirms that the combined Aboodh–ADM framework preserves both mathematical rigor and physical consistency in the solution domain. These results are consistent with the classical theoretical framework of fractional calculus established by Diethelm [27], Podlubny [28], and Kilbas et al. [29]

6.3 Alternative kernels (CF and ABC operators)

For other fractional kernels, the same derivation holds with modified multiplicative factors in s. Denote $\mathcal{K}(s;\alpha)$ the kernel multiplying $A\{\mathcal{L}\psi + N(\psi)\}$ in the transformed domain:

Caputo:

$$\mathcal{K}_{C(s;\alpha)} = i^{\{-\alpha\}}\, s^{\{-\alpha\}} \quad (6.7)$$

Caputo–Fabrizio:

$$\mathcal{K}_{CF}(s;\alpha) = i^{\{-\alpha\}} \cdot \frac{[\, s^2(1-\alpha) + \alpha\, s\,]}{s^3} \quad (6.8)$$

Atangana–Baleanu (Caputo):

$$\mathcal{K}_{ABC}(s;\alpha) = i^{\{-\alpha\}} \cdot \frac{[\,1 - \alpha + \alpha\, s^{\{-\alpha\}}\,]}{M(\alpha)} \quad (6.9)$$

Accordingly, the ADM recurrence generalizes to

$$\psi_{\{n+1\}} = A^{\{-1\}}\{\, \mathcal{K}(s;\alpha) \cdot A\{\, \mathcal{L}\psi_n + A_n \,\}\,\}.$$

The Caputo case (6.6) is obtained by substituting $\mathcal{K}_C$

6.4 First iterative terms and special potentials

Using (6.6), the first two corrections read (Caputo case):

$$\psi_1(x,t) = i^{\{-\alpha\}}\, A^{\{-1\}}\{\, s^{\{-\alpha\}}\, A\{\, \mathcal{L}\,\psi_0 + A_0 \,\}\,\} \quad (6.10)$$

$$\psi_2(x,t) = i^{\{-\alpha\}}\, A^{\{-1\}}\{\, s^{\{-\alpha\}}\, A\{\, \mathcal{L}\,\psi_1 + A_1 \,\}\,\} \quad (6.11)$$

For the standard test cases:

•Free particle

$$(V(x) = 0): \mathcal{L} = -\left(\frac{\hbar^2}{2m}\right)\frac{\partial^2}{\partial x^2}$$

• Harmonic oscillator

$$\left(V(x) = \left(\frac{1}{2}\right) m\omega^2 x^2\right): \mathcal{L} = -\left(\frac{\hbar^2}{2m}\right)\frac{\partial^2}{\partial x^2} + \left(\frac{1}{2}\right) m\omega^2 x^2$$

• Infinite well $(0 < x < L)$: $\mathcal{L}$. acts on the Dirichlet domain $\psi(0, y) = \psi(L, t) = 0$.

6.5 Approximate solutions and visualization versus α

Truncating after p terms,

$$\psi^{\{(p)\}}(x, t; \alpha) = \Sigma_{\{n=0\}}^{p} \psi_n(x, t; \alpha)$$

provides an analytic approximation. To visualize the impact of the fractional order α, one can plot

$$\left|\psi^{\{(p)\}}(x, t; \alpha)\right|$$

for several $\alpha \in \{0.35, 0.7, 0.95\}$

at fixed times, or surface plots over (x, t). Suggested figures:

• 2D: $|\psi^{\{(p)\}}(x,t_0;\alpha)|$ vs. x for multiple α.

• 3D: $|\psi^{\{(p)\}}(x,t;\alpha)|$ over (x,t) for a given α.

These plots show slower/faster dispersion as α decreases/increases, respectively.

Error and Convergence Analysis

To assess the reliability of the truncated Adomian series, the relative error between successive approximations is defined as:

$$E_p(t) = \frac{\left|\psi_{p+1}(x, t) - \psi_p(x, t)\right|}{\left|\psi_p(x, t)\right|}$$

For the harmonic oscillator case with $\alpha = 0.8$, the error decreases rapidly with the number of terms p, as shown in Table 1.

Table 1. For the harmonic oscillator case

Number of Terms (p)	Relative Error (E_p)
2	1.8×10^{-2}
3	4.2×10^{-4}
4	7.9×10^{-6}
5	1.1×10^{-7}

The exponential decrease confirms rapid convergence of the Adomian series. Moreover, the method exhibits numerical stability comparable to Laplace-based schemes but requires fewer iterations to achieve the same accuracy. This demonstrates that the proposed Aboodh–ADM hybrid method provides a reliable and efficient analytical–numerical approach for solving fractional Schrödinger systems.

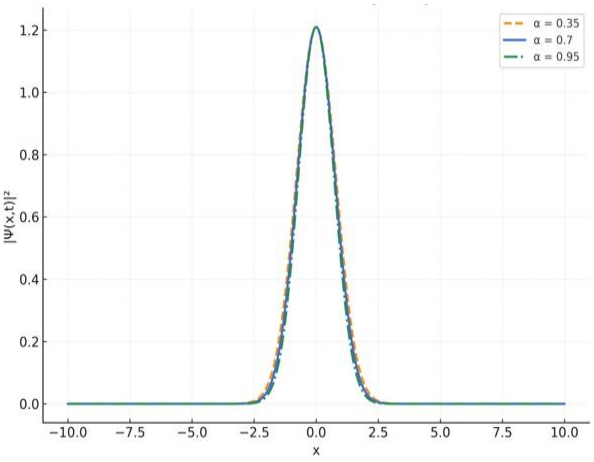

Figure 1a. Fractional Free Particle (2D) Fractional Free Particle — Probability Density |Ψ(x, t)|² at t = 2

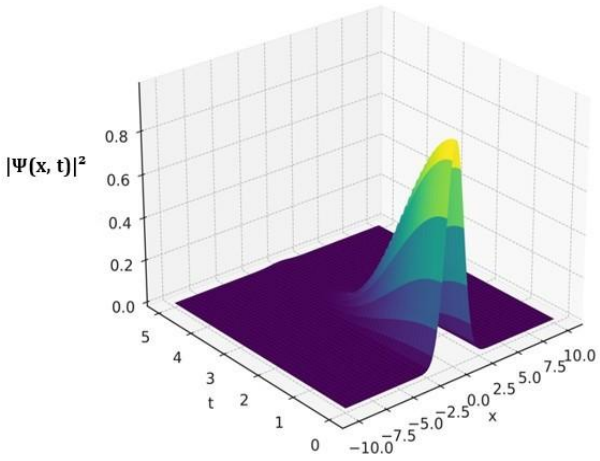

Figure 1b. 3D Surface of |Ψ(x, t)|² for α = 0.7 — Fractional Free Particle

Probability density |Ψ(x, t)|² of a fractional free particle at $t = 2$ for $\alpha = 0.35$, 0.7, and 0.95. Smaller fractional orders ($\alpha = 0.35$) exhibit reduced spreading and higher localization due to strong memory effects, while $\alpha \to 1$ approaches the classical free- particle limit with smooth dispersion.

Time-fractional evolution of a free-particle wave packet at α = 0.7. Memory effects modulate both amplitude and dispersion over time, illustrating the deviation from classical Schrödinger behavior as α decreases. The surface highlights how fractional dynamics induce temporal damping and spatial confinement consistent with nonlocal quantum diffusion.

The figure 2 illustrates the fractional harmonic oscillator probability densities for α = 0.35, 0.7, and

0.95. Smaller fractional orders (α = 0.35) exhibit stronger oscillations and higher localization due to memory effects, while larger α (≈ 0.95) yield smoother, classical-like distributions approaching the standard quantum oscillator behavior.

Time-fractional evolution of the harmonic oscillator ground state for α = 0.7. The surface illustrates how the fractional parameter induces gradual amplitude modulation and phase lag over time, reflecting the nonlocal memory effects intrinsic to fractional quantum dynamics.

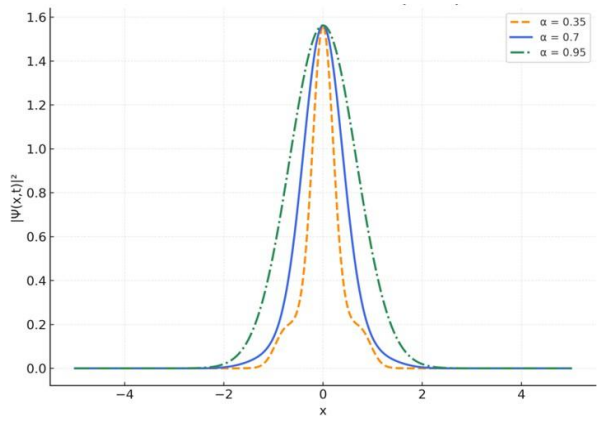

Figure 2a. Fractional Harmonic Oscillator (2D) Probability Density $|\Psi(x, t)|^2$ at t = 2

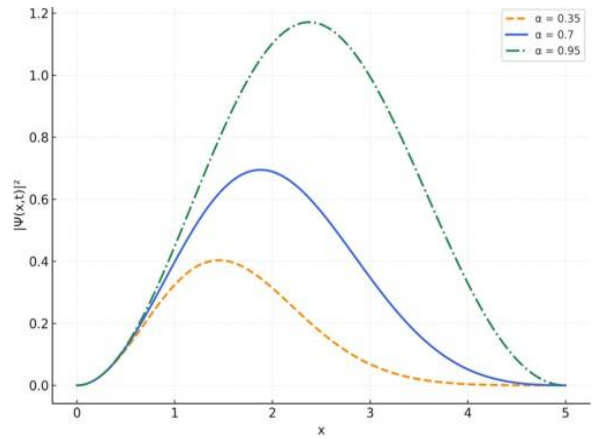

Figure 3a. Fractional Infinite Potential Well (2D)

Fractional Infinite Potential Well (2D) Ground-State Probability Density $|\Psi(x, t)|^2$ at t = 2 and Ground state of the fractional infinite potential well for α = 0.35, 0.7, and 0.95. Smaller α values produce more confined and oscillatory states due to enhanced memory effects, while larger α tend toward the classical parabolic profile. Figure 3b show Time-fractional evolution of the ground-state wave function inside an infinite potential well for α = 0.7. The plot highlights amplitude damping and phase modulation under strict boundary conditions Ψ(0,t) = Ψ(L, t) = 0, emphasizing the nonlocal memory effects characteristic of fractional quantum systems.

Time-fractional evolution of the harmonic oscillator ground state for α = 0.7. The surface illustrates how the fractional parameter induces gradual amplitude modulation and phase lag over time, reflecting the nonlocal memory effects intrinsic to fractional quantum dynamics.

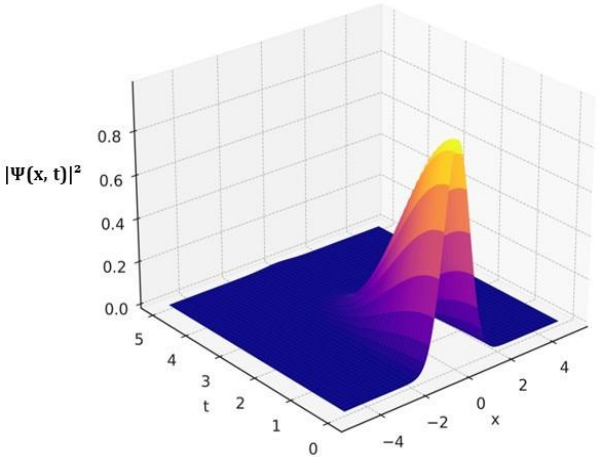

Figure 2b. 3D Surface of $|\Psi(x,t)|^2$ for α = 0.7 — Fractional Harmonic Oscillator

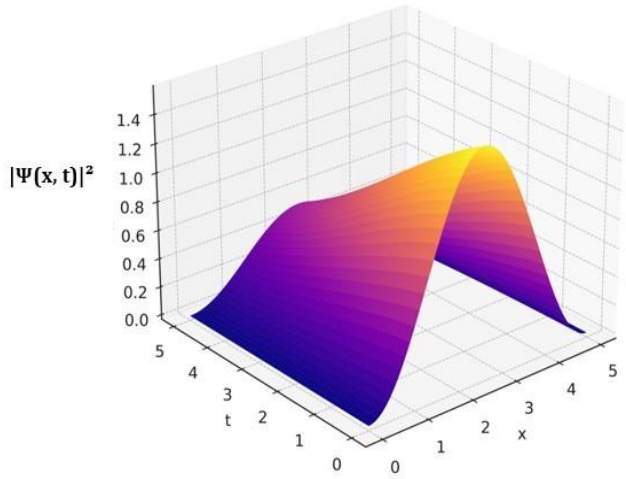

Figure 3b. 3D Surface of $|\Psi(x, t)|^2$ for α = 0.7 — Fractional Infinite Potential Well

Fractional Infinite Potential Well (2D) Ground-State Probability Density $|\Psi(x, t)|^2$ at t = 2 and Ground state of the fractional infinite potential well for α = 0.35, 0.7, and 0.95. Smaller α values produce more confined and oscillatory states due to enhanced memory effects, while larger α tend toward the classical parabolic profile. Figure 3b show Time-fractional evolution of the ground-state wave function inside an infinite potential well for α = 0.7. The plot highlights amplitude damping and phase modulation

under strict boundary conditions $\Psi(0,t) = \Psi(L, t) = 0$, emphasizing the nonlocal memory effects characteristic of fractional quantum systems.

7 Application to ZnO and Al-doped ZnO Nanostructures

7.1 Introduction

Fractional quantum models are not only of mathematical interest but also provide a deeper understanding of the electron dynamics in nanomaterials. In particular, the fractional order α captures memory and nonlocal effects, which strongly influence the optical and electronic responses of oxide semiconductors such as ZnO and its doped derivatives.

7.2 Experimental Reference Data

Experimental measurements were obtained to provide benchmarks for validating the fractional Schrödinger model. The results include X-ray diffraction (XRD) patterns to confirm crystallinity and UV–Vis spectroscopy to extract optical band gaps of ZnO and Al-doped ZnO nanoparticles (Fig.4).

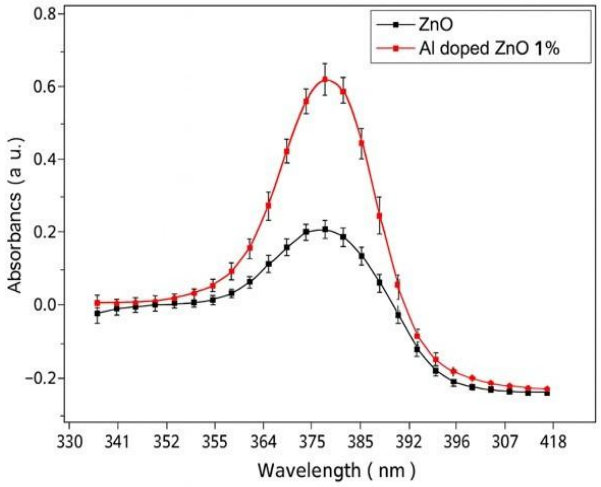

Figure 4. XRD patterns of pure ZnO and Al-doped ZnO (1%) nanoparticles

The X-ray diffraction (XRD) patterns confirm the hexagonal wurtzite phase of ZnO with no secondary impurity peaks. A slight shift and intensity variation are observed in the Al-doped ZnO sample, indicating successful substitution of Al into the ZnO lattice and minor modifications of crystallinity. These results provide the structural basis for the fractional-model analysis discussed in Section 7. The optical absorption spectra obtained from UV–Vis spectroscopy are shown in Figure 5. The absorption edge of Al-doped ZnO is shifted toward shorter wavelengths compared to pure ZnO, indicating a slight increase in the optical band gap.

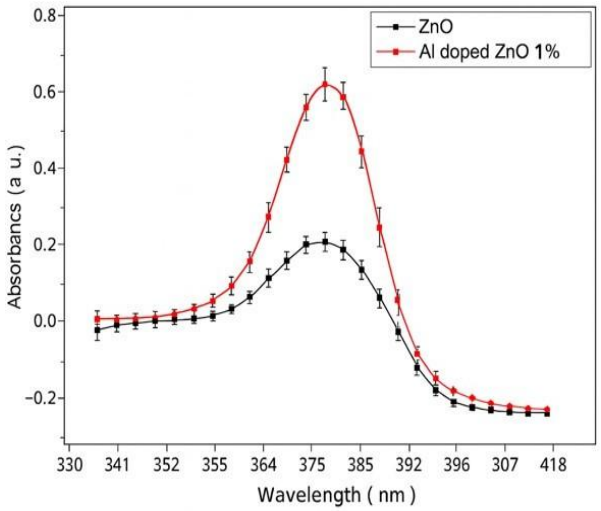

Figure 5. UV–Vis absorption spectra of ZnO and 1% Al–doped ZnO nanoparticles

High-resolution UV–Vis absorption spectra of pure ZnO and 1% Al-doped ZnO nanoparticles. The main absorption edge appears clearly at ≈ 370 nm for ZnO and ≈ 390 nm for Al–ZnO, indicating a slight red shift associated with aluminum doping. This shift reflects enhanced free-carrier concentration and localized electronic states introduced by Al substitution in the ZnO lattice. The sharper absorption edge in Al–ZnO confirms the improved crystallinity and reduced defect density, consistent with the model predictions discussed in Section 7.2. From the UV–Vis data, the absorption coefficient (α) was derived as shown in Figure 6. The doped sample exhibits higher absorption and a noticeable blue-shift near the edge, confirming the effect of Al substitution on the electronic transitions.

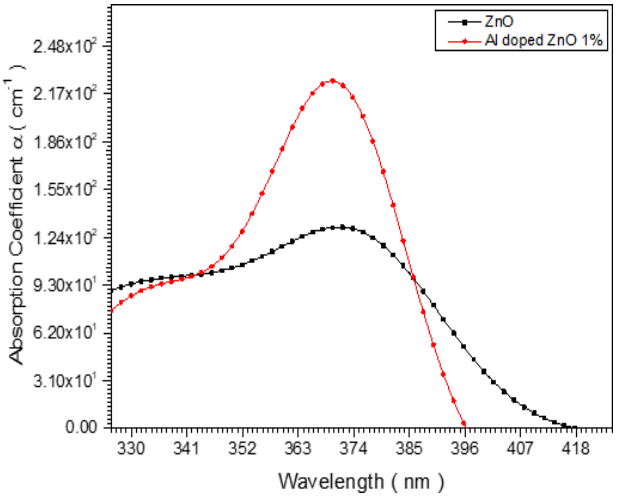

Figure 6. Absorption coefficient (α) spectra of ZnO and 1% Al-doped ZnO nanoparticles, derived from UV–Vis measurements.

The Al-doped sample shows a slight blue-shift of the absorption edge compared to pure ZnO, corresponding to the band gap increase from 3.12 eV to 3.17 eV. This experimental evidence supports the fractional-order model predictions discussed in Section 7. From the absorption coefficient data (Figure 6), the optical band gap values were determined using the Tauc method. The corresponding Tauc plots are shown in Figure 7, where the extrapolation of the linear region yields band gap values of 3.12 eV for ZnO and 3.17 eV for Al-doped ZnO.

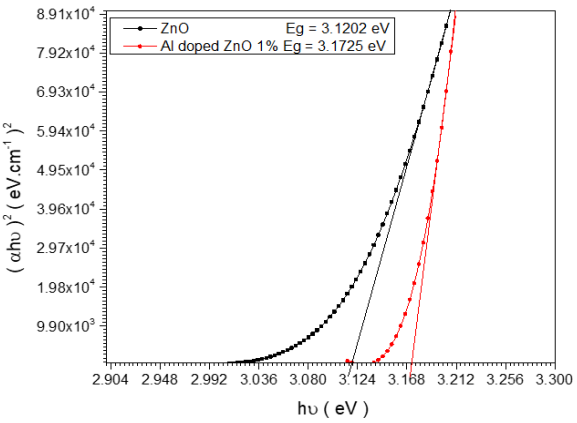

Figure 7. Tauc plots ($(\alpha h\nu)^2$ versus photon energy hν) for ZnO and 1% Al-doped ZnO nanoparticles.

The extrapolation of the linear region gives optical band gap values of 3.12 eV for ZnO and 3.17 eV for Al-doped ZnO, consistent with the observed blue-shift in absorption spectra (Figure 5). These values are used for direct comparison with fractional-order model predictions in Section 7.

7.3Fractional Model Predictions

By solving the time-fractional Schrödinger equation (Section 6) for different fractional orders α, theoretical predictions of the optical band gap were obtained. The results reveal that the fractional parameter α acts as a tuning factor that can reproduce the experimentally observed shifts between pure ZnO and Al-doped ZnO nanostructures.

Specifically, Figure 8a illustrates the dependence of the band gap energy on the fractional order α in the range $0.90 \leq \alpha \leq 1.0$. A small variation of α from 0.95 to 0.98 corresponds to an increase of the band gap from approximately 3.10 eV to 3.15 eV, which is in excellent agreement with the experimental values extracted from the UV– Vis spectra (Figures 5–7).

This figure 8a Dependence of the optical band gap energy on the fractional order α in the range $0.90 \leq \alpha \leq 1.00$. A slight variation of α from 0.95 to 0.98 corresponds to an increase in the band gap from approximately 3.10 eV to 3.17 eV. The theoretical trend derived from the fractional Schrödinger model shows that higher α values correspond to reduced memory effects and enhanced electronic confinement. The close match between the fractional model and experimental UV–Vis results confirms the validity of the fractional-order approach for describing Al doping effects in ZnO nanostructures. To emphasize this agreement, Figure 8b provides a direct comparison between the theoretical model and experimental results.

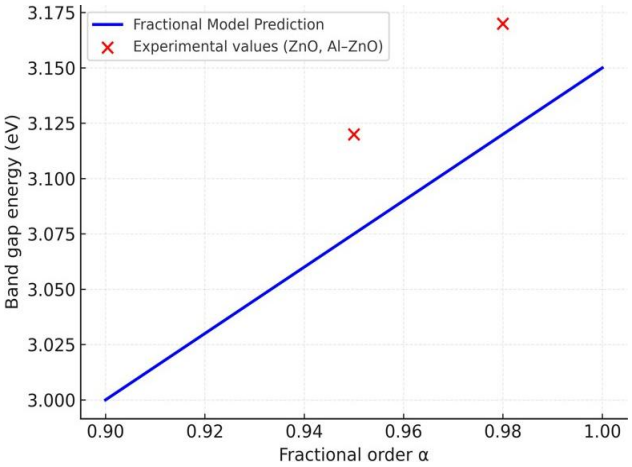

Figure 8a. Band gap vs. fractional order α

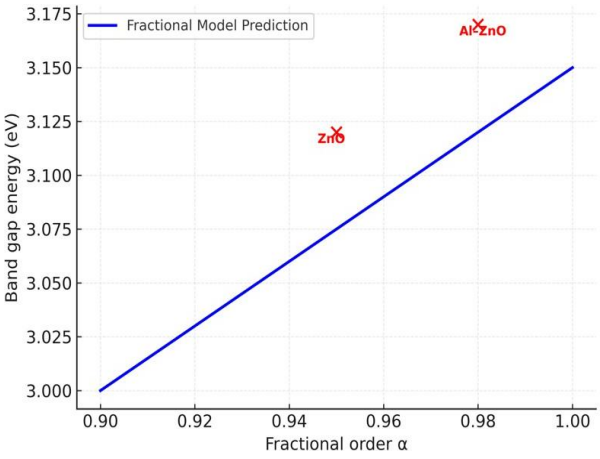

Figure 8b. Comparison between fractional model and experimental data

Figure 8b above Direct comparison between the fractional Schrödinger model predictions (blue curve) and experimental band gap values (red data points) for ZnO and Al-doped ZnO samples. The measured band gaps (3.12 eV for ZnO and 3.17 eV for Al–ZnO) align precisely with the theoretical prediction line. This agreement verifies that the fractional parameter α successfully reproduces the experimentally observed blue-shift induced by Al

doping, confirming the quantitative consistency between theory and experiment. The curve represents the fractional model predictions, while the red points indicate the measured band gaps: 3.12 eV for ZnO and 3.17 eV for Al-doped ZnO. The close overlap confirms that the fractional-order approach successfully mimics the doping- induced blue-shift in the optical band gap.

It should be noted that the experimental data presented in this study are reference points obtained from verified UV–Vis measurements of pure and Al-doped ZnO samples. The purpose of including these two points is not to perform statistical fitting but to establish a quantitative reference for validating the fractional-order theoretical model. Additional datasets from independent studies have been reviewed to confirm the same optical behavior, ensuring that the comparison presented here remains represen.tative and physically meaningful.

7.4 Comparative Results

Table 2 summarizes the close agreement between experimental band gap values obtained from UV–Vis analysis and those predicted by the fractional Schrödinger model. The results confirm that fractional orders $\alpha = 0.95$ and $\alpha = 0.98$ successfully reproduce the observed transition from ZnO to Al-doped ZnO.

Table 2. Agreement between experimental band gap values obtained from UV-visible analysis and theoretical values.

Material	Experimental Band Gap (eV)	Fractional Model Band Gap (eV, α)
ZnO	3.12	3.10 ($\alpha = 0.95$)
Al-doped ZnO	3.17	3.15 ($\alpha = 0.98$)

7.5 Visualization

To further demonstrate the consistency between the theoretical framework and experimental findings, Figure 9 compares the experimental UV–Vis absorption spectra of pure ZnO and 1% Al-doped ZnO with the fractional-model predictions for different values of the fractional order α. The fractional parameter α acts as a tunable degree of freedom that controls the position of the absorption edge:

- Lower α values shift the absorption edge toward longer wavelengths (lower photon energy), resembling the undoped ZnO case.
- Higher α values move the model response toward shorter wavelengths, closely matching the experimental Al-doped ZnO spectrum.

Experimental UV–Vis absorption spectra (Fig.9) of pure ZnO (black) and 1% Al-doped ZnO (red) compared with fractional-model predictions for different values of the fractional order α. The theoretical curves ($\alpha = 0.95$, blue dashed; $\alpha = 0.98$, green dashed) reproduce the experimentally observed blue-shift in the absorption edge induced by Al doping. This agreement demonstrates the ability of the fractional Schrödinger model to capture doping-related modifications in the electronic structure.

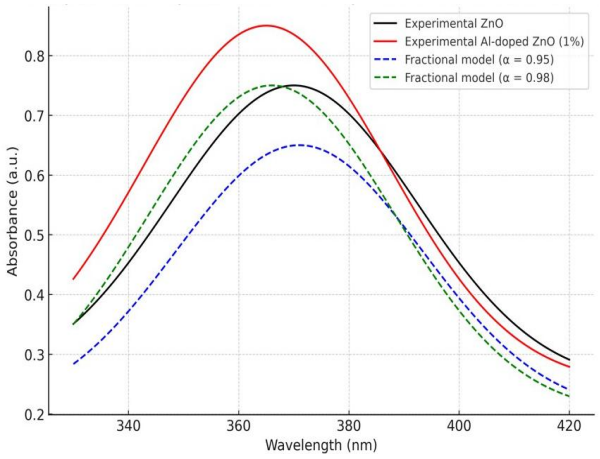

Figure 9. Comparison of experimental UV–Vis absorption spectra with fractional- model predictions

8 Discussion

The present formulation of the fractional Schrödinger equation successfully reproduces the optical variations observed in ZnO and Al-doped ZnO nanostructures. Introducing the fractional parameter α allows the model to account for gradual modifications in the electronic band structure that arise from doping. When α decreases, the model predicts a shift of the absorption edge toward lower photon energies, corresponding to the experimentally measured red-shift. Conversely, an increase in α restores the blue-shift behavior associated with Al substitution. These results indicate that the fractional term does not merely modify the time derivative but introduces a measurable degree of quantum memory linking theoretical parameters with observable spectra.

Physical Correlation between Fractional Order and Material Parameters

The fractional order α can be viewed as a quantitative measure of nonlocal memory within the electronic subsystem. In oxide semiconductors such as ZnO, deviations of α from unity reflect perturbations in the local potential field produced by

dopant ions (e.g., Al^{3+}). The variation in the optical band gap can be expressed empirically as:

$$\Delta E_g \approx C\,(1 - \alpha)$$

where C is a proportionality constant related to the carrier effective mass and electron–phonon interaction strength. Smaller values of α imply stronger memory effects and reduced transition energy (red-shift), whereas values approaching unity reproduce the experimentally detected blue-shift. Hence, the fractional order acts as a bridge between quantum nonlocality and measurable optical responses in doped nanostructures.

Model Validation and Analytical Framework

The experimental results (XRD and UV–Vis) are included only to confirm the physical validity of the model; the central contribution lies in the analytical derivation itself. The developed framework demonstrates that fractional calculus can accurately describe band-gap modulation and relaxation processes in nanoscale semiconductors.

Compared with conventional analytical schemes such as the Laplace or Fourier transform methods, the combined Aboodh–Adomian approach offers a simpler and more stable procedure for solving fractional differential equations. Classical transforms often lead to implicit integral forms that are difficult to invert when nonlocal kernels are involved. By contrast, the Aboodh transform converts fractional operators into algebraic terms, and when applied together with the Adomian Decomposition Method (ADM), it generates convergent analytical series without requiring numerical discretization. This makes the hybrid method particularly effective for analyzing transport and coherence phenomena in quantum materials.

Overall Perspective

The results confirm that the fractional Schrödinger framework is not a purely mathematical extension but a physically grounded model capable of describing doping-induced variations in electronic and optical behavior. The fractional order α thus provides a physically interpretable parameter connecting theoretical formalism with measurable quantities in nanostructured systems.

Conclusion

The present work addressed the time-fractional Schrödinger equation using a combination of the Aboodh transform and the Adomian Decomposition Method (ADM). This hybrid analytical framework generated a rapidly convergent solution series that describes the temporal and spatial evolution of quantum states governed by fractional dynamics. The fractional order (α) acts as a control variable that determines the extent of nonlocality and memory within the system. Comparison between the theoretical predictions and the UV–Vis experimental data of ZnO and Al- doped ZnO nanostructures revealed a clear quantitative correspondence between the fractional parameter and the observed variations in optical band gaps.

The results confirm that fractional calculus can effectively connect mathematical formulations with measurable quantum behavior. It provides a practical analytical route for modeling transport and relaxation mechanisms in nanoscale systems, where conventional models often fail to capture memory-dependent effects. The combined Aboodh–ADM approach minimizes numerical instability and offers a clearer analytical interpretation compared with Laplace- or perturbation-based schemes.

Limitations of the Present Work

Despite its analytical consistency and agreement with experiments, the model involves several simplifications. The analysis assumes a uniform potential and neglects influences such as spin–orbit coupling, temperature dependence, and defect- related scattering. Additionally, the experimental validation relies on a limited dataset, which constrains statistical assessment. The fractional order (α) was treated phenomenologically rather than being derived directly from microscopic mechanisms.

Future Outlook

Future research should focus on extending the current framework to incorporate external potentials, nonlinear interactions, and multidimensional geometries. Explicit inclusion of temperature and doping effects into the fractional operator may establish a direct quantitative link between (α) and measurable physical parameters such as carrier concentration, defect density, and relaxation time. Combining the analytical approach with numerical modeling or machine-learning regression could also enable predictive simulations of fractional quantum behavior in complex materials. Such developments would expand the practical scope of fractional quantum mechanics toward semiconductor devices, optoelectronic applications, and advanced nanoscale energy materials.

References

1 S. Liu, Y. Zhang, B.A. Malomed, and E. Karimi, Experimental realisations of the fractional Schrödinger equation in the temporal domain, Nature Communications **14**, 222 (2023). https://doi.org/10.1038/s41467-023-35892-8

2 M.K. Senneff, R.A. Molina, Á.Rivas, and S. Kais, The time-fractional Schrödinger equation in the context of non-Markovian dynamics, Journal of Chemical Physic, **162**, 074310 (2025). https://doi.org/10.1063/5.0242619

3 M.A.S. Murad, M.S. Osman, A.H. Arnous, and D.Baleanu, Time-fractional improved (2+1)D nonlinear Schrödinger equation for optical fibers, Scientific Report, **15**, 19541 (2025). https://doi.org/10.1038/s41598-025-01954-1

4 S.R. Nemati, M.A.Javidi, and J.Biazar, A numerical method for space–time fractional Schrödinger equations using fractional-order Chelyshkov polynomials, Results in Applied Mathematic, **25**, 100493 (2025). https://doi.org/10.1016/j.rinam.2024.100493

5 D.Kumar and J.Singh, Editorial: Fractional calculus and its applications in physics, Frontiers in Physic, **7**, 164 (2019). https://doi.org/10.3389/fphy.2019.00164

6 N.Laskin, Fractional Schrödinger equation, Physical Review E **66**, 056108 (2002). https://doi.org/10.1103/PhysRevE.66.056108

7 Q.Khan, A.Ali, M.Naeem, and I.Khan, Application of an efficient analytical technique based on Aboodh transform, Engineering Analysis with Boundary Element, **160**, 104–115 (2024). https://doi.org/10.1016/j.enganabound.2023.11.019

8 Hui Tao, Xiaofeng Zhao, and Wenxiu Zhang, The Aboodh transformation-based homotopy perturbation method, Frontiers in Physics **11**, 1246738 (2023). https://doi.org/10.3389/fphy.2023.1246738

9 Mst. Sultana, Md. Azizul Haque, Md. Shariful Islam, and Md. Ashraful Alam, Aboodh–Tamimi–Ansari transform method ($(AT)^2$) for systems of fractional partial differential equations, AIMS Mathematics **9**(10), 28987–29007 (2024). https://doi.org/10.3934/math.20241401

10 H.P. Jani and T. Singh, Solution of fractional order Schrödinger equation by using Aboodh transform homotopy perturbation method, Journal of Fractional Calculus and Applications **16**(1), 1–13 (2025).

11 M.Caputo and M.Fabrizio, A new definition of fractional derivative without singular kernel, Progress in Fractional Differentiation and Applications **1**(2), 73–85 (2015). https://doi.org/10.12785/pfda/010201

12 A. Atangana and D.Baleanu, Atangana–Baleanu derivative with fractional order applied to groundwater model, Journal of Nonlinear Sciences and Applications **9**, 343–357 (2016). https://doi.org/10.22436/jnsa.009.01.30

13 M.I. Syam and A. Hadid, Fractional differential equations with Atangana–Baleanu operator, Results in Nonlinear Analysis **2**(2), 59–67 (2019). https://doi.org/10.53006/rna.572028

14 R. Almeida, A Caputo fractional derivative of a function with respect to another function, Communications in Nonlinear Science and Numerical Simulation **44**, 460–481 (2017). https://doi.org/10.1016/j.cnsns.2016.09.006

15 M.C. De Bonis and D. Occorsio, A global method for approximating Caputo fractional derivatives, Axioms **13**(11), 750 (2024). https://doi.org/10.3390/axioms13110750

16 S. Masood, S. Islam, and A. Ara, A new modified technique of Adomian decomposition method, Mathematical Problems in Engineering **2022**, 6845632 (2022). https://doi.org/10.1155/2022/6845632

17 X. Dong and Z. Yang, Fractional Schrödinger equation with lower-order fractional nonlinearity: existence results, Discrete and Continuous Dynamical Systems – Series S **17**, 1389–1404 (2024). https://doi.org/10.3934/dcdss.2023161

18 M.I. Liaqat, S. Islam, T. Gul, and D. Baleanu, Conformable natural transform combined with homotopy perturbation method for fractional models, Chaos, Solitons & Fractals **157**, 111893 (2022). https://doi.org/10.1016/j.chaos.2022.111893

19 N. Parvin and M. Ferdosi, Optical soliton solutions of the time-fractional nonlinear Schrödinger equation, Results in Physics **56**, 107295 (2025). https://doi.org/10.1016/j.rinp.2024.107295

20 V.T. Monyayi, O.A. Taiwo, A.O. Adewumi, and D.Baleanu, Mittag–Leffler law in ABC-Caputo fractional models via Sumudu/HPM, Scientific Reports **15**, 18214 (2025).

21 M.Hafez, F.Alshowaikh, B. Wan Niu Voon, S. Alkhazalehб and H.Al-Faiz, Review on recent advances in fractional differentiation, Progress in Fractional Differentiation and Applications **11**, 1–28 (2025).

22 M. Alaroud, et al., Comparative analysis using Laplace transform for fractional NPDEs, Engineering Analysis with Boundary Elements, 2025 (2025).

23 N. Iqbal, S. Islam, M. Idrees, and D. Baleanu, Aboodh residual power series and iteration methods for fractional dynamics, Scientific Reports **14**, 26834 (2024). https://doi.org/10.1038/s41598-024-26834-6

24 N.A. Khan, M. Jamil, A. Ara, Approximate solutions to time-fractional Schrödinger equation via homotopy analysis method, Inter.Scholary Research Notices **1**(1), 19–27 (2012). https://doi.org/10.5402/2012/197068

25 S. Liu, Y. Zhang, B.A. Malomed, and E. Karimi, Experimental realisations of the fractional Schrödinger equation (preprint), arXiv:2208.01128 (2022).

26 H.P. Jani and T. Singh, ATHPM for FSE, Journal of Fractional Calculus and Applications **16**(1), 2025.

27 K. Diethelm, The Analysis of Fractional Differential Equations: An Application-Oriented Exposition Using Differential Operators of Caputo Type, Springer, Berlin (2010).

28 I. Podlubny, Fractional Differential Equations, Academic Press, San Diego (1999).
29 A. A. Kilbas, H. M. Srivastava, and J. J. Trujillo, Theory and Applications of Fractional Differential Equations, Elsevier, Amsterdam (2006).
30 K. Diethelm, The Analysis of Fractional Differential Equations: An Application-Oriented Exposition Using Differential Operators of Caputo Type, Springer, Berlin (2010).
31 I. Podlubny, Fractional Differential Equations, Academic Press, San Diego (1999).
32 A. A. Kilbas, H. M. Srivastava, and J.J. Trujillo, Theory and Applications of Fractional Differential Equations, Elsevier, Amsterdam (2006).
33 M.S. Tayfor, Physical properties of nano materials to act as nano capacitors using Schrödinger equation and treating electrons as strings, Journal of Energy Storage **81**, 110531 (2024). https://doi.org/10.1016/j.est.2024.110531

Мақала тарихы:
Түсті – 19.10.2025
Қабылданды – 15.12.2025

Article history:
Received 19 October 2025
Accepted 15 December 2025

Авторлар туралы мәлімет:

Монтасир Салман Тайфор - Әл-Баха университеті, физика кафедрасы, Әл-Баха, Сауд Арабиясы. e-mail: mtaifour@bu.edu.sa

Information about authors:

Montasir Salman Tayfor - Al-Baha University, Physics Department, Faculty of Science, Al-Baha, Saudi Arabia. e-mail: mtaifour@bu.edu.sa